Journal of the Electrochemical Society, 1992, Volume 139, Issue 7, Pages 1812-1820.
ISSN: 0013-4651
DOI: 10.1149/1.2069503
http://www.electrochem.org/
http://scitation.aip.org/getpdf/servlet/GetPDFServlet?filetype=pdf&id=JESOAN000139000007001812000001&idtype=cvips&prog=normal

X-Ray Absorption Study of Electrochemically Grown Oxide Films on Al-Cr Sputtered Alloys

I. *Ex situ* Studies

G. S. Frankel*
IBM Research Division, T. J. Watson Research Center, Yorktown Heights, New York.

A. J. Davenport* and H. S. Isaacs*
Brookhaven National Laboratory, Division of Applied Sciences, Upton, New York.

A. G. Schrott, C. V. Jahnes, and M. A. Russak
IBM Research Division, T. J. Watson Research Center, Yorktown Heights, New York.
* Electrochemical Society Active Member.

ABSTRACT

Oxides grown electrochemically in a borate buffer solution on the surface of sputter-deposited AlCr alloy films were studied by x-ray absorption near edge structure (XANES). The measurements were made in air immediately following polarization in solution. The oxides were also examined with x-ray photoelectron spectroscopy (XPS). The effects of alloy composition and thickness as well as applied potential were studied. Cr(VI) was found in the oxides if the applied potential was sufficiently high. The Cr(VI) was enriched at the interface with the electrolyte and the proportion of Cr(VI) in the oxide was higher for alloy films containing more Cr. The Cr(VI) in the oxides could be reversibly reduced to Cr(III) and reoxidized to Cr(VI) by subsequent potentiostatic treatments in solution.

The nature of Cr in anodic films on metals is of great interest due to its ability to confer corrosion resistance. While numerous techniques exist for examining elements in oxide films, x-ray absorption near edge structure (XANES) and extended x-ray absorption fine structure (EXAFS) have been shown to be extremely useful for deriving information regarding valence and coordination in passive films (1-4).

Incorporation of Cr into anodic films on Al has been studied previously with XANES (5, 6). Hawkins *et al*. investigated the uptake of Cr upon exposure at open circuit to a chromate solution by Al which had been previously anodized in borate (5). They found Cr in both the 3^+ and 6^+ oxidation states with larger relative amounts of Cr(VI) in thicker anodic oxides, *i.e.*, those

anodized to a higher voltage. In contrast, a sample supporting only an air-formed oxide contained only Cr(III) after immersion in chromate solution. They suggested that Cr(VI) adsorbed on the oxide surface and reduction of Cr(VI) to Cr(III) accompanied dissolution of Al at the base of flaws in the oxide film. Thicker oxides had fewer flaws and thus showed more Cr in the 6^+ state.

Recent work by Chung et al. (6) explored the uptake of Cr by Al anodized directly in chromate electrolytes. Cr(VI) was found to be incorporated into the growing oxide following adsorption at the surface. The absolute amount of Cr(VI) in the films was independent of formation voltage, but the amount of Cr(III) increased uniformly with oxide film thickness. The oxide was profiled by making x-ray absorption measurements following dissolution for varying times in sulfuric acid. The 6^+ state was found to be associated with the outer surface, Cr(III) was enriched in the bulk of the oxide, and the region of oxide nearest the metal was found to be devoid of Cr. These observations were supported by cross-sectional transmission electron micrographs. It was suggested that the Cr(VI) anions in the near-surface region are reduced by the field in the oxide to form mobile Cr(III) cations which then move back toward the surface under the influence of the field.

In the present investigation, XANES was used to study Cr in oxides formed by polarizing AlCr alloys in an aqueous solution. Cr was thus introduced into the oxides from the metallic state rather than from the solution as chromate. AlCr alloys have been shown to be quite resistant to pitting corrosion in chloride solutions, although not as resistant as other Al binary alloys (7,8). It has been suggested that the onset of pitting in AlCr alloys was associated with transformation of Cr in the oxide from Cr(III) to Cr(VI) at about −200 mV SCE which is well below the equilibrium potential for Cr(VI) formation (7).

The x-ray absorption measurements in this study were carried out at glancing angle to enhance surface sensitivity. They were made *ex situ* in air following the polarization treatments. We have reported similar measurements made *in situ* in an electrochemical cell (9,10) but this report will focus on the ex situ experiments. Another *ex situ* technique, x-ray photoelectron spectroscopy (XPS), was also used to characterize the oxide films formed on the AlCr alloys. It will be shown that the XPS data are supportive of and complementary to the XANES data.

Experimental

Samples.—AlCr alloy films for the x-ray absorption studies were sputter-deposited onto 2.5 cm × 5.1 cm × 0.6 cm float glass substrates. Alloys with 4, 20, 32, and 46% Cr and thicknesses of 20, 40, 70, 150, and 1500 Å were tested. Very thin alloy layers were studied in an attempt to reduce the chromium signal from underlying metal. Since the AlCr alloy layer thickness was quite small, and the films were possibly not continuous in some cases, a 1000-2000 Å underlayer of sputter-deposited Nb was used to ensure electrical contact to all regions of the film during polarization. The Nb underlayer exhibited hillocks approximately 500 Å in diameter as observed by scanning electron microscopy (SEM). The AlCr alloy layers were then sputter-deposited on top of the Nb without breaking vacuum. A composite target composed of either Cr pins in an Al target or pure Al foil partially overlaid on a Cr target was used so as to produce samples with spatially uniform compositions. The compositions were determined by Rutherford backscattering (RBS) analysis of films deposited onto carbon substrates in the same deposition run.

Sample preparation.—Half of the sample was immersed in a beaker of 0.5*M* H_3BO_3 +

0.05M $Na_2B_4O_7$ with a pH of 7.36. A mercurous sulfate reference electrode (MSE, 0.64 V *vs.* SHE) was used and all potentials will be referred to MSE. Following 1 min at open circuit, the potential was stepped to either −0.5, 0.7, 2, or 5 V and held for 5 min. The samples were then washed in water, dried under a stream of Ar, and transferred to the beam line for analysis. The measurements took approximately 20 min per sample.

XANES experiments.—The valence of Cr in these polarized films was studied by glancing angle x-ray absorption experiments at the Cr K edge which is at 5989 eV. The x-ray energy in the XANES experiments is always referred to the Cr edge at 5989 eV in this work. The x-ray absorption of the anodic films on the alloys was determined by monitoring the fluorescent radiation, I_f, using an ionization chamber placed directly above the sample, Fig. la. The incident, I_0, and reflected beam intensity, I_r were measured by ionization chambers located to either side of the sample. I_r/I_0 was used as a measure of the absorption coefficient. A K_2CrO_4 powder standard placed in front of a final ionization chamber generated I_{ref}, a reference signal for monitoring monochrometer drift.

The experiments were performed *ex situ* in air directly following electrochemical polarization. Following alignment of the sample surface in the x-ray beam, the incident angle θ was varied from 0-10 mrad at a fixed beam energy of 25 eV above the Cr edge. Figure 1 b, a typical angle scan, shows both x-ray reflection and absorption (as indicated by fluorescence). At the critical angle for total external reflection, about 5 mrad in Fig. 1 b, the reflected radiation drops dramatically and the fluorescent radiation increases due to an increase in penetration of x-rays into the sample. By comparing the absorption edges taken at angles above and below the critical angle for a given condition, it is possible to estimate the distribution of Cr species in the

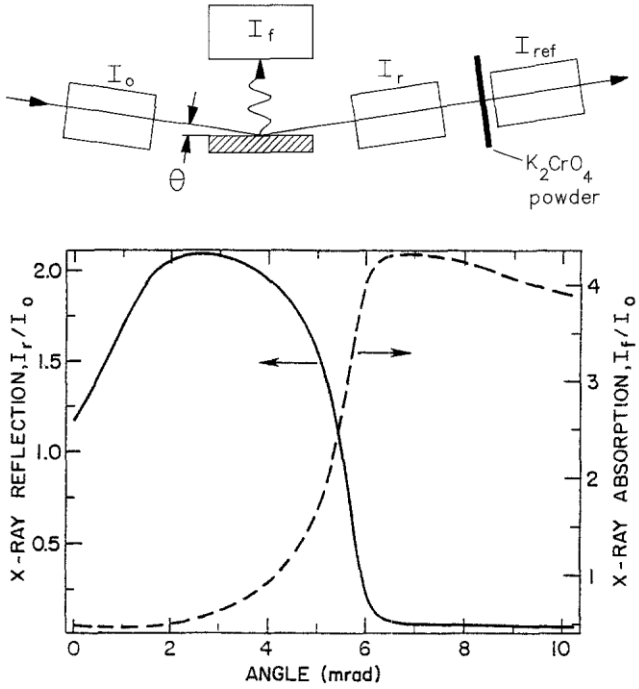

Fig. 1. (a, top) Schematic of glancing angle experimental setup, (b, bottom) X-ray reflection and absorption

(determined by fluorescence) as a function of incident angle for a typical sample.

oxide film. An energy scan made below the critical angle is more surface sensitive than at a high angle where the x-rays penetrate more deeply into the sample. The energy scans were generally from -30 to +50 eV relative to the Cr edge at an angle above and below the critical angle using a step size of 0.5 eV and an integration time of 1 s. For the case shown in Fig. 1, energy scans were made at 4 and 6 mrad. The experiments were performed on beam lines X11A and X23A2 at the National Synchrotron Light Source.

The background below each edge was extrapolated above the edge and subtracted. The absorption coefficients were normalized to result in a unit step height at 50 eV above the edge. While the edge structure may influence the signal at +50 eV and normalization should be done at a higher energy, +50 eV was the energy limit of most scans.

Measurements of Cr metal foil and powdered Cr-containing compounds were made in transmission for use as reference standards. The absorption coefficient for the transmission experiments was In (I_0/I_t) where I_0 and I_t were measured by ionization chambers located to either side of the samples. Alloy films approximately 1 μm thick were deposited onto 4 μm thick Mylar sheets for determination of the absorption spectra characteristic of Cr in the metallic alloys. Several sheets together were measured in the transmission mode. These thicker films had 2.8, 12, 23, 36.6, and 48% Cr and were thus slightly different in composition than the thin films used to form the anodic oxides. These experiments were performed at a later date than the others and the energy scans were extended to +200 eV to facilitate normalization.

XPS studies.—Some of the samples studied by XANES were later studied by XPS. Other samples were freshly prepared in an identical fashion. The samples first studied by XANES had been exposed to air for several days before introduction into the XPS chamber. Freshly prepared samples were introduced into the high vacuum XPS chamber within 5 min of the polarization treatment. We observed no degradation of the oxides during the longer exposure to air. Monochromatized Al Ka radiation was used since it has been shown to minimize photodecomposition compared to the nonmonochromatic source (11). The energy positions of the photoemission peaks were corrected for charging with the C Is line at 284.6 eV which is due to adventitious carbon.

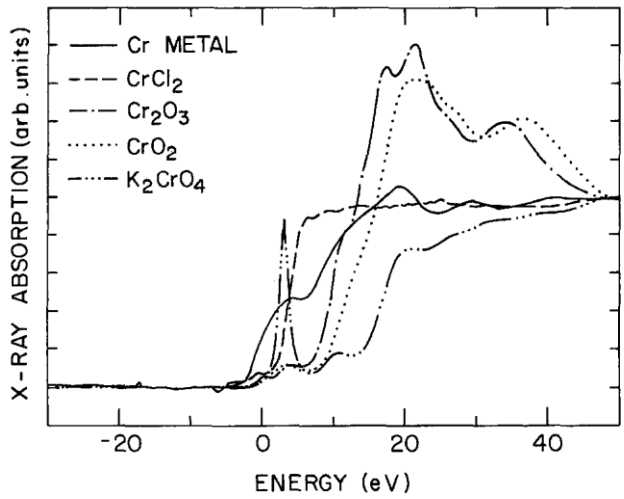

Fig. 2. Absorption edges of reference standards relative to the Cr K edge at 5989 eV.

Results

XANES data.—Absorption spectra for reference standards of varying Cr valence are shown in Fig. 2. There is a monotonic shift in the position of the edge to higher energies as the valence of the Cr species increases. The edge position is thus a clear indication of valence. A distinct pre-edge peak at 3 eV equal in height to the edge is associated with Cr (VI) compounds. This feature has been attributed to transitions to a bound antibonding state which are allowed by the tetrahedral coordination of chromate (12). As a result of this peak and the edge shift, a small amount of hexavalent Cr in a compound of mixed valence is readily observed in the absorption edge. Cr_2O_3 and CrO_2 have characteristic peaks directly at the top of the edge followed by a decrease in intensity over the next 50 eV. The metallic Cr foil displays a shoulder halfway up the edge which is characteristic of many metals (13).

Absorption edges for the thick alloy films and pure Cr foil measured in transmission are given in Fig. 3. Also shown in Fig. 3 are the edges measured from powdered samples of the intermetallic alloys Cr_2Al and $CrAl_7$. The edges for the alloys comprise a smooth transition from one intermetallic to the other. The major peak on the edge is approximately at the same energy (25 eV) and about 6 eV above the major edge peak for pure Cr.

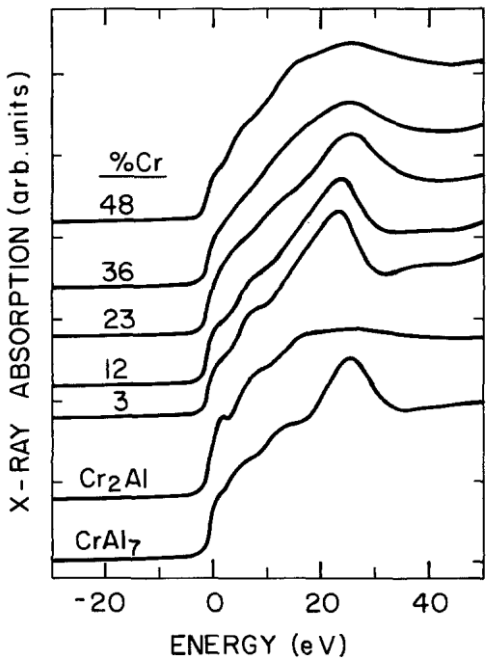

Fig. 3. Absorption edges of thick alloy films on Mylar and powdered Cr_2Al and $CrAl_7$ intermetallics measured in transmission.

The normalized spectra of the oxide films were fitted using a least squares nonlinear regression analysis to a sum of Cr(0), Cr(III), and Cr(VI) reference standards. K_2CrO_4 and Cr_2O_3 were used as the Cr(VI) and Cr(III) standards, respectively. As the energy limit of the absorption edges taken for the oxide standards was rather close to the edge itself, the standards were normalized for fitting by determining multiplicative factors that resulted in accurate fitting of data taken on mixtures of known amounts of K_2CrO_4 and Cr_2O_3 powders. The Cr(0) standard was the absorption spectrum measured in transmission for each of the alloy compositions. Cr(IV) was assumed not to be present in these oxide films as the fits were typically quite good with $r^2 > 0.98$ using only Cr(0), Cr(III), and Cr(VI) standdards. By separating the spectra of the oxide films into zero-, three-, and six-valent components in this fashion, it is possible to determine the fraction of the signal from oxidized Cr (which is related to oxide thickness for a given angle) and the fraction of Cr(VI) in the oxide. By comparing data to composite edges prepared by linear addition of the standards in various combinations, it was determined that the computational accuracy of the fitted values is approximately ±5%. The real accuracy is also limited by slight differences in the actual spectra of the Cr(III) and Cr(IV) constituents of the films from those of the standard compounds. However, the fits use real spectra in contrast to the hypothetical line shapes used to fit XPS data. A further limitation on the accuracy of the fits is due to anomalous dispersion. The penetration depth of x-rays depends upon the absorption coefficient which varies abruptly at the edge (14). Therefore, in the edge region, the penetration depth is poorly defined. While this may distort the ratio of oxidized to metallic Cr for the thick alloy films, it does not affect the measurements made on the thinnest films.

Figure 4 through Fig. 7 summarize the effects of alloy composition, alloy thickness, and applied potential on the fraction of oxidized Cr and the proportion of Cr(VI). For all cases, spectra above and below the critical angle were analyzed.

The fraction of oxidized Cr is shown in Fig. 4 as a function of potential and alloy composition for 40 Å thick alloy films. The percent oxide is taken to be the sum of the contributions due to Cr(III) and Cr(VI). The percent oxidized Cr increases with potential

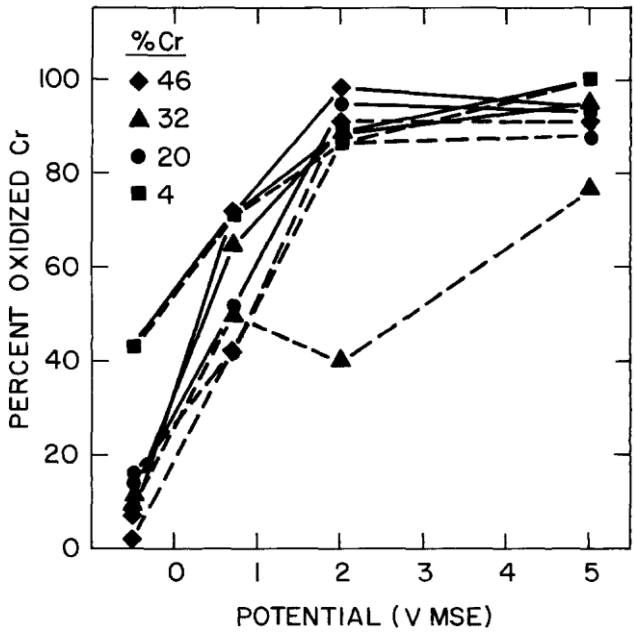

Fig. 4. Influence of alloy film composition and applied potential on total oxidized Cr [sum of Cr(lll) and Cr(VI) components] for 40 Å thick alloy films. As described in the text, however, the 32% film was 60 Å thick. Solid and dashed lines represent measurements made with incident angle below and above the critical angle, respectively.

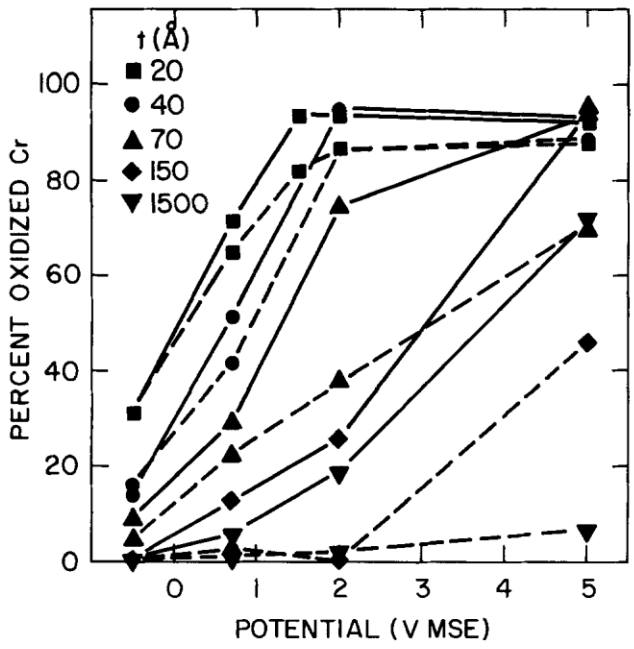

Fig. 5. Influence of alloy film thickness and applied potential on total oxidized Cr (sum of Cr(lll) and Cr(VI) components) for 20% Cr films. Solid and dashed lines represent measurements made with incident angle below and above the critical angle, respectively.

reaching 90-100% for all compositions as the potential reaches 2 V. In all cases, more metallic Cr is measured at angles above the critical angle which reflects the lower penetration depth of x-rays below the critical angle. The 32% Cr samples showed substantially less oxidized Cr or more metallic Cr above the critical angle than the other compositions. These samples were approximately 60 Å thick and were thus somewhat thicker than the others. As will be presently described, alloy thickness influences the percent oxidized Cr measured. The 70 Å films with 20% Cr are seen in Fig. 5 to be similar to the 32% Cr samples in Fig. 4.

The proportion of the signal from oxidized Cr is larger for alloy films with a smaller deposited thickness. In other words, the contribution of underlying metallic Cr increases with increasing alloy thickness. This is shown for 20% Cr alloys in Fig. 5. The absorption edges for

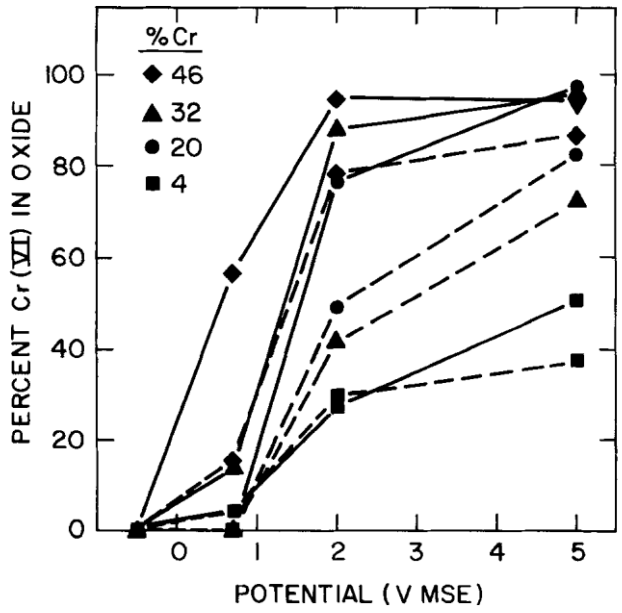

Fig. 6. Influence of alloy film composition and applied potential on Cr(VI) content in oxide for 40 Å thick alloy films. Solid and dashed lines represent measurements made with incident angle below and above the critical angle, respectively.

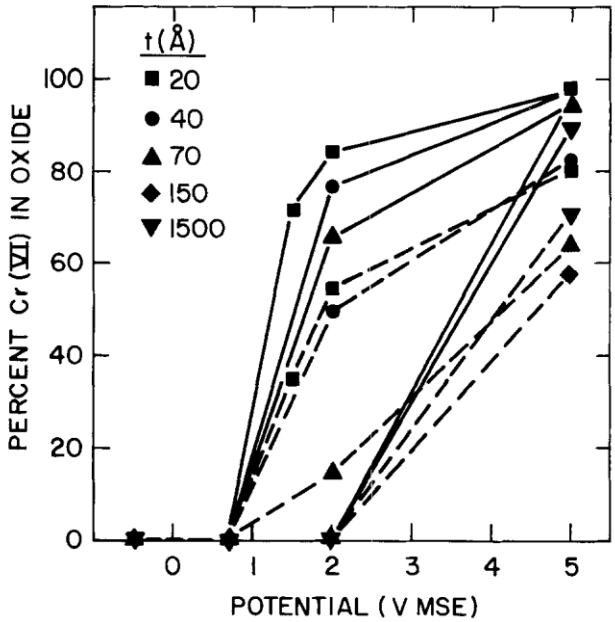

Fig. 7. Influence of alloy film thickness and applied potential on Cr(VI) content in oxide for 20% Cr films. Solid and dashed lines represent measurements made with incident angle below and above the critical angle, respectively.

20% Cr films polarized at −0.5 V are given in Fig. 8. The fit for the 20 A film edge yielded 31% Cr(III) and 69% Cr(0). As the alloy thickness increased to 1500 Å, the Cr(0) content of the signal increased so that the edge looked close to that for a pure metallic sample even at incident angles below the critical angle. At the highest potential studied, 5 V, all thicknesses except the 1500 Å film exhibit a signal below the critical angle that is mostly oxidized Cr.

The fraction of Cr(VI) in the oxide is a strong function of both applied potential and alloy composition, Fig. 6. No chromate was observed for any of the films polarized at −0.5 V as all of the oxidized Cr was in the 3^+ state. At higher potentials, progressively more of the Cr was converted to Cr(VI). The spectra in Fig. 9 show that for the 40 Å thick films with 20% Cr the

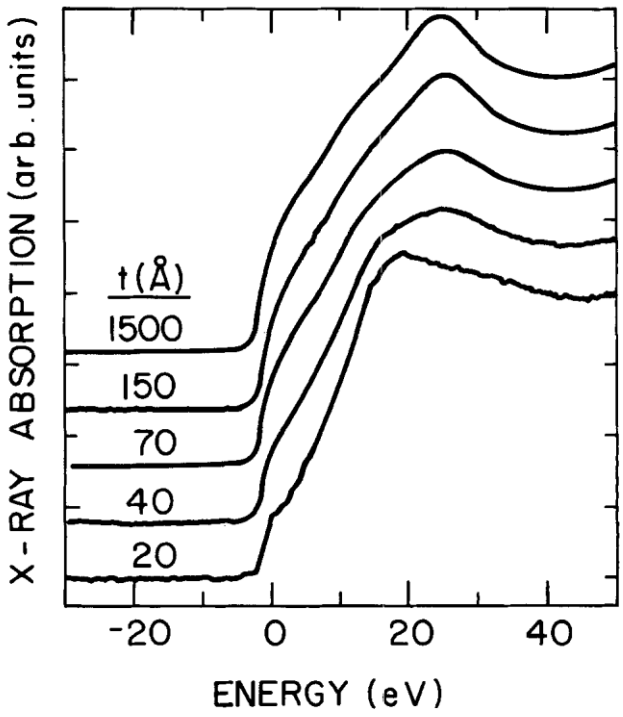

Fig. 8. Influence of alloy film thickness on absorption edges for 20% Cr films polarized at -0.5 V MSE, measured below the critical angle.

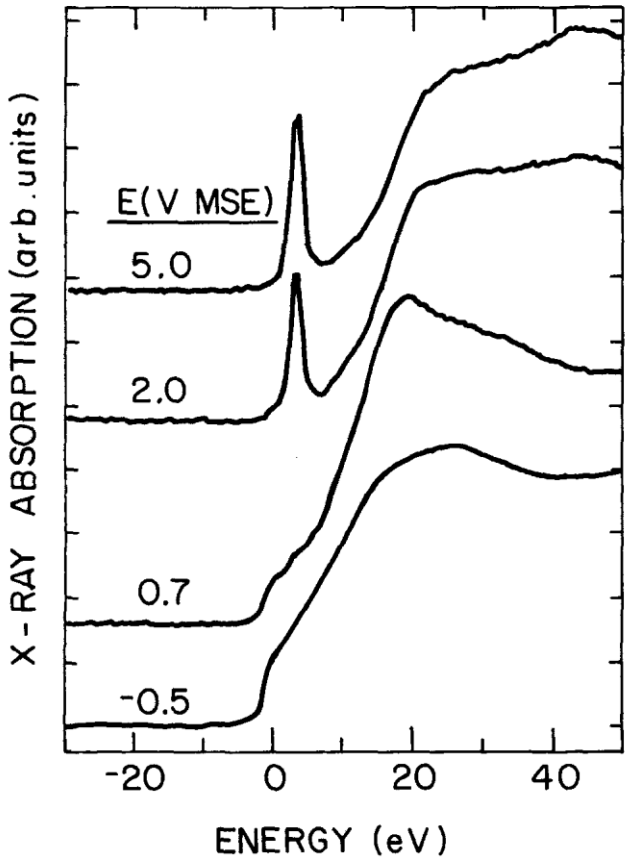

Fig. 9. Influence of applied potential on absorption edges for 20% Cr 40 Å films, measured below the critical angle.

edges move to higher energy and the pre-edge peak becomes more prominent as the potential is increased. The 4 and 20% Cr alloys exhibited essentially no evidence of Cr(VI) until 2 V while the 32 and 46% Cr films had pre-edge peaks at 0.7 V as well. The effect of alloy concentration on the Cr valence in the oxide is shown in Fig. 10 for 40 Å thick alloy films polarized to 2 V. There is a steady increase in the pre-edge peak height as the Cr concentration increases.

The thickness of the alloy film is shown in Fig. 7 to affect the observed valence of Cr in the oxide. More Cr(VI) is detected in oxides on thinner alloy films than on thicker alloy films for a polarization potential of 2 V. The spectra in Fig. 11 for 20% Cr alloys exhibit this phenomenon. Signal from the underlying metal results in a characteristic shoulder at 0 eV for the 1500 and 150 Å films. However, these spectra exhibit little evidence of the pre-edge peak at 3 eV associated with chromate while the 20, 40, and 70 Å films all have large pre-edge peaks. The thicker films showed evidence of Cr(VI) only at 5 V.

XPS data.—The Al 2p and Cr 3p XPS peaks for 40 Å thick, as-received, air oxidized alloy samples are shown in Fig. 12 with the energy corrected for charging using the adventitious C peak at 284.6 eV. The Al 2p line for oxidized Al always fell at 74 eV which is in agreement with that expected for $A1_20_3$ (15). Curves a to d in Fig. 12 correspond to alloy concentrations of 5, 20, 32, 43% Cr, respectively, as determined by RBS. The Cr concentrations determined from

the Cr/Al XPS peak area ratios (oxidized + metallic) are 1.5, 12, 25, and 44% Cr, respectively. These values are lower than the bulk values, with the exception of the highest Cr concentration alloy. Furthermore, the ratio of metallic to oxidized Cr is much larger than that for Al at all concentrations. These observations indicate that the Cr in the alloy tends to be protected by preferential surface segregation and oxidation of Al. The discrepancy between RBS and XPS is larger as the alloy Cr concentration decreases. The ratio of metallic to oxidized peak heights for both Al and Cr decreases as the Cr concentration decreases, indicating a thicker oxide film. So the ambient-formed oxide is both thicker and more enriched with Al for lower Cr concentration alloys.

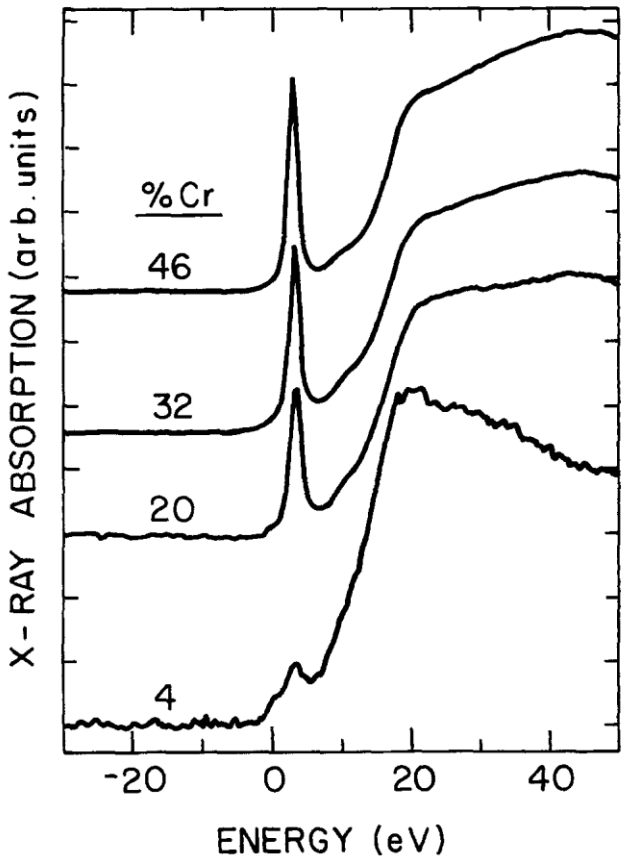

Fig. 10. Influence of alloy composition on absorption edges for 40 Å films polarized at 2 V MSE, measured below the critical angle.

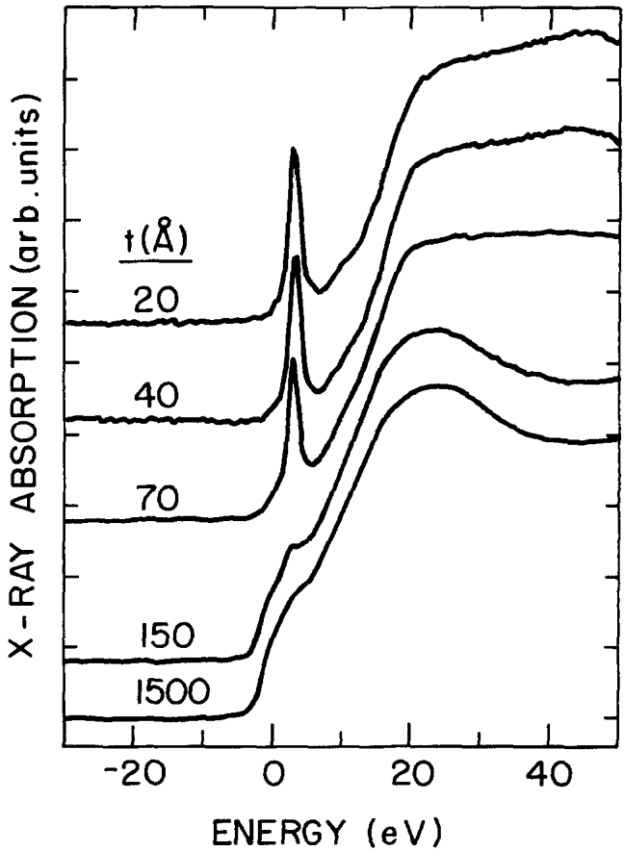

Fig. 11. Influence of alloy film thickness on absorption edges for 20% Cr films polarized at 2 V MSE, measured below the critical angle.

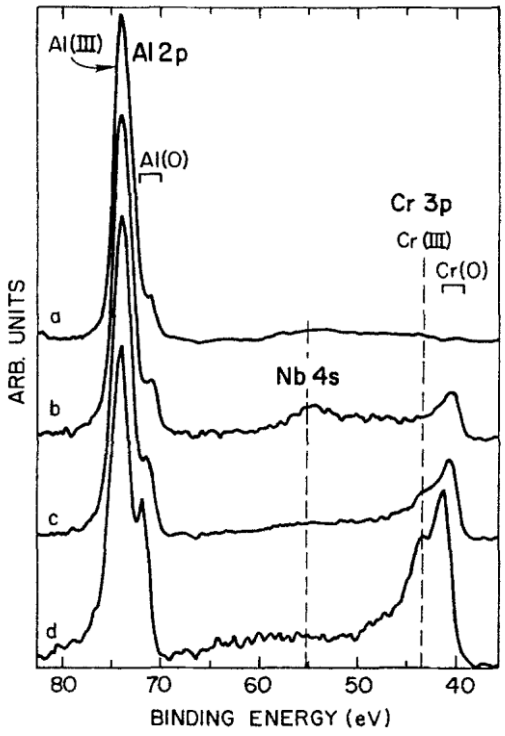

Fig. 12. XPS spectra for as received 40 Å films with bulk alloy compositions of a, 5%; b, 20%; c, 32%, and d, 43% Cr. The spectra are normalized to the height of the Al(lll) peak.

The Al and Cr metallic peaks shift to higher binding energy as the Cr concentration increases in Fig. 12. This observation may be explained by charging which is observed even for thin oxides on metals during photo-emission. As a result of this charging, the oxide and the adventitious C on the oxide surface (used as a reference) are at a more positive potential than the underlying metal which is electrically connected to the spectrometer and is therefore not charged. In Fig. 12, the alloys with less Cr are seen to have a thicker native oxide. Since thicker oxide films may sustain a larger charge, our referencing method results in an apparent shift towards lower binding energies for the metallic components of both Cr and Al as the Cr concentration decreases. This is an artifact and not representative of a true shift in binding energy upon alloying (16).

The XPS spectra obtained after polarization of the alloy samples at 5 V agreed with the XANES results in that the Cr is in the 6^+ oxidation state. Figure 13 shows spectra following polarization for the same nominal compositions as in Fig. 12. Curves a to d exhibit a Cr 3p peak corresponding mainly to Cr(VI). It is interesting to observe a similar Cr to Al peak area ratio on the order of 10% for curves b-d in Fig. 13.

The XPS peak around 60 eV for curves a and b in Fig. 13 and around 54 eV for curves a and b in Fig. 12 corresponds to the 4s line for Nb which is the conductive underlayer. The Nb is metallic in the as-received condition (17) implying that the coverage of the alloy is complete for a 40 Å thick film. The metallic Nb is sensed through thin regions of the overlying alloy. The thickness of the metallic alloy through which this Nb peak can be seen is three times the mean-free path or, for this electron kinetic energy, approximately 35 Å (18). However, for wide bandgap insulating oxides, the mean-free path could be two times larger (19). Since the Nb

signal is only observed at the lowest Cr concentrations, the wetting of the alloy film on the Nb under-layer apparently improves as the Cr content increases so that less thin alloy areas are exposed. The Nb peak in Fig. 13 suggests that the Nb is oxidized following polarization to 5 V. Identification of the oxidation state of Nb in this figure is complicated by the possibility that this oxide is defective and thus conductive. Artifacts due to charging similar to those described above for Cr are likely to occur.

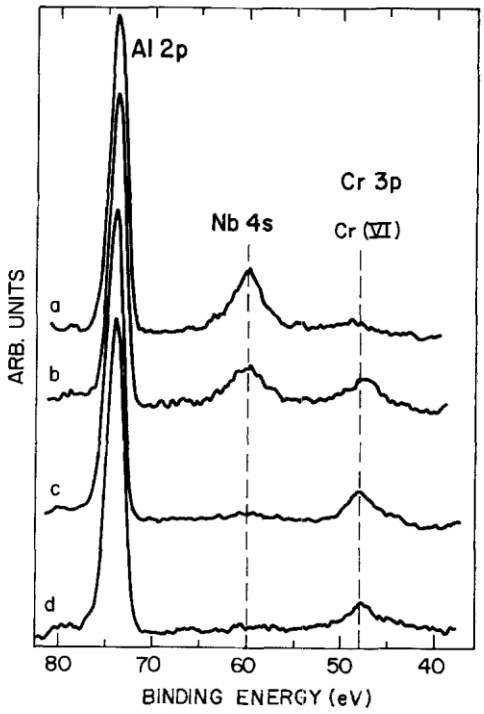

Fig. 13. XPS spectra for 40 Å films polarized to 5 V with bulk alloy compositions of a, 5%; b, 20%, c, 32%, and d, 43% Cr. The spectra are normalized to the height of the Al(lll) peak.

Figure 14 displays the effect of polarization potential for 40 Å thick Al-43% Cr films. The trends of increased oxidation state and oxide thickness observed with XANES are also seen in this figure. Curve a corresponds to −0.5 V and is identical to that of the air-formed oxide. As a result of oxide thickening, curves b to d do not exhibit metallic Cr although a small amount of metallic Al is seen at 0.7 V, curve b. The amount Cr(III) decreases with polarization potential above 0.7 V as in the XANES results. The shoulder at 48 eV in curve a of Fig. 14 and curve d of Fig. 12 is due to a satellite of the 3p peak of Cr(III) and not to Cr(VI).

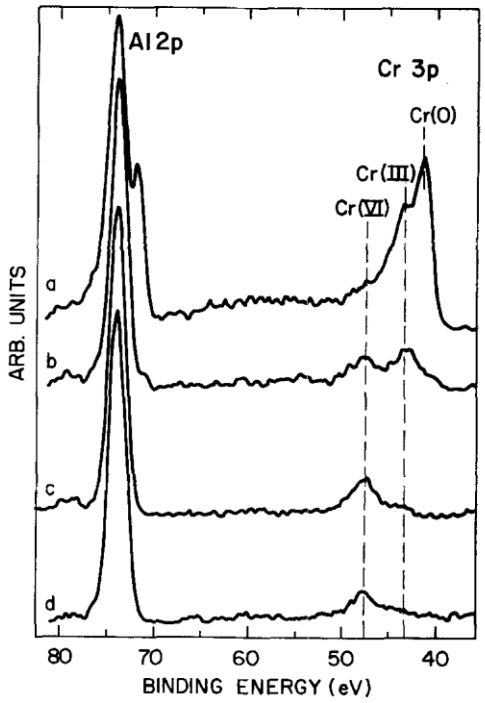

Fig. 14. XPS spectra for 40 Å 43% Cr films polarized at a, 0.5; b, 0.7; c, 2; and d, 5 V. The spectra are normalized to the height of the Al(lll) peak.

This is verified by analysis of the corresponding Cr 2p peaks which are not shown. The area corresponding to the Cr 3p peak in the 6^{+} state is roughly equivalent for curves b to d which is similar to that seen in Fig. 13. The total amount of Cr(VI) is apparently independent of potential and alloy composition.

Discussion

Anodized Al has many technological uses. It is of interest to understand the nature of the anodized oxide and the processes tacking place therein. In this study, the behavior of Cr in anodized Al oxides is investigated using two x-ray techniques. The x-ray absorption technique is a sensitive means for detection of the oxidation state of Cr in oxide films. Cr is particularly suitable for this analysis due to the relatively large separation between the zero-, three-, and six-valent edges as well as the characteristic Cr(VI) pre-edge peak. A major advantage of the technique is the ability to make measurements in air or in solution. The emphasis in this study was to use XANES measurements to quantify the relative amounts of the various Cr oxidation states. Comparison of the absolute amount of Cr in the films under glancing angle conditions is less accurate due to the possibility of slight variations in the footprint of the beam on the sample surface from run to run if the incident angle is slightly different.

While both techniques have good surface sensitivity, XPS has advantages and disadvantages *vis-a-vis* XANES. XPS peaks have better energy resolution, and it is possible to collect data in a wide energy range so that different elements can be probed in the same experiment. However, ultrahigh vacuum is required for XPS and analysis is complicated by

sample charging, final state relaxation effects, and features such as satellites. Data collection times are also much longer than for XANES. In combination, these two techniques reveal considerable information regarding the nature of Cr in the oxide films on AlCr alloys.

The oxidation state of the Cr increases with potential in accordance with thermodynamic principles. The equilibrium potentials at pH 7.4 for Cr/Cr_2O_3 and Cr_2O_3/CrO_4^{2-} are −1.091 and 0.558 V SHE (−1.731 and −0.082 V MSE), respectively (20). Through deconvolution of Cr 2p XPS spectra, Moshier et *al.* found that 34% of the oxidized Cr was in the +6 state for a Al-14% Cr alloy polarized in KC1 to −0.247 V SCE (−0.643 V MSE) (7). Furthermore, they indicated the presence of some Cr(VI) for this alloy even at -0.6 V SCE (−0.996 V MSE). While direct comparison to the work of Moshier *et al*. is not possible since different electrolytes were used, there was no indication in the present work of the formation of Cr(VI) at −0.5 V MSE, the only potential studied below the equilibrium potential. Cr(VI) was, however, found to be present in the oxides if the applied potential was at or above 0.7 V MSE. The *in situ* experiments provided better electrochemical control and more detailed information regarding the critical potential for Cr(VI) formation (10). That work found that 0.2 V MSE was the lowest potential at which Cr(VI) was observed. This value is 0.3 V above the equilibrium potential.

Other investigators have found Cr(VI) in oxides on Al formed by exposing anodized Al to chromate solution (5) or by anodizing Al directly in chromate solution (6). In those studies, it could be claimed that the chromate was either adsorbed from solution or entrapped in the growing oxide so that it was not really a stable part of the oxide film. In the present study, the Cr(VI) in the oxide was not formed by adsorption or entrapment of chromate from solution. Rather, it came from Cr in the alloy and remained incorporated in the oxide despite the extremely high solubility of chromate in the aqueous phase.

Comparison of the measurements made with incident singles above and below the critical angle show that, when present, there is always a higher concentration of Cr(VI) in the outer region of the oxide near the solution compared to the "bulk" of the oxide. It has been observed that the passive films on many metals consist of a bilayer or at least contain a valency gradient with the higher valent cations found in the outer part of the oxide which is closer to the interface

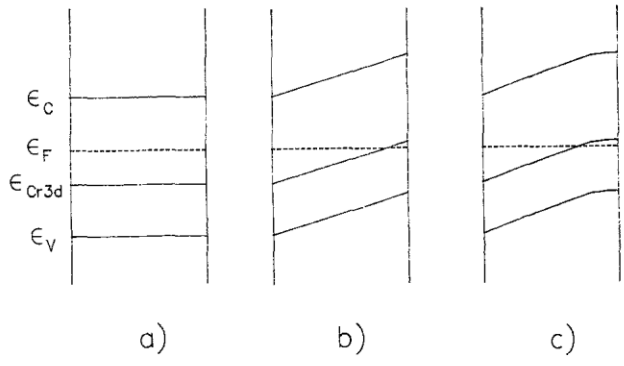

Fig. 15. Electron energy band diagram for Al_20_3 containing Cr-ion impurities. ε_c and ε_v, indicate the bottom of the conduction band and lop of the valence band for Al_2O_3, ε_F is the Fermi level, (a) flatband condition, (bj band tilting due to applied anodic potential, (c) additional band bending due to existence of chromate anions in surface region.

with the environment (21). These observations have been explained using a simple semiconductor electron band model (21, 22). According to cluster calculations, the presence of Cr in $A1_2O_3$ modifies the band structure in the flatband condition by introducing occupied localized states in the bandgap of $A1_2O_3$ at about 4 eV from the top of the valence band (23). This level is indicated in Fig. 15a as ε_{Cr3d}- Anodic polarization produces an upward tilt of the bandgap, Fig. 15b, and oxidation of Cr(III) to Cr(VI) is thermodynamically possible when the Fermi level becomes lower than the electron level of the oxidation reaction (21, 22). As a result of the band tilting, the oxidation occurs first at the outer surface. Very clear evidence for this process is seen in the behavior of Cr in these oxide films.

The Cr content in the alloy film influences the measured proportion of Cr(VT) as is shown in Fig. 6 and Fig. 10. The existance of chromate anions in the oxide film alters the energy bands beyond the tilting created by the applied anodic potential. The excess negative charge associated with the chromate near the surface makes it an accumulation region, similar to that described for a p-type semiconductor (24, 25). This will produce a negative band bending at the interface with the electrolyte. Since the sample is held at a fixed potential, the end points of the bands are pinned and the band assumes a curvature shown in Fig. 15c. The net effect is to move the intersection of the Fermi level with the Cr 3d level to a point deeper in the film, and thus resulting in additional chromate formation. Since the curvature of the band increases with the number of acceptors states (24) which in this case is chromate ions, it is reasonable to assume that the higher the initial concentration of Cr, the higher the curvature and thus the higher the ratio of Cr(VI) to CrGII) for a fixed polarization potential, which is in agreement with experiment. It should be noted that this description of the oxide is for the system after polarization for 5 min at a given potential.

The study of chromium chemistry in anodic oxides necessitated the use of very thin alloy layers to reduce the x-ray fluorescence contribution from the Cr in the alloy. Typically the thickness of the underlying metal would not be expected to affect the surface oxide thickness or the oxidation state of the ions in the oxide. The ability of the x-rays to penetrate the oxide and the alloy must, however, be taken into account. At the Cr edge, the 1/*e* penetration depth of x-rays is approximately 30 Å for incident angles below the critical angle and thousands of angstroms for incident angles above the critical angle (4). Therefore, above the critical angle the x-rays probe the entire thickness of the oxide and underlying metal while the outer 30 Å should dominate the measurements made below the critical angle. However, the samples in the present study were very thin alloy films on substrates that were rough on the scale of the thickness of the alloy layers. As a result, parts of the surface were above the critical angle even when the incident angle was below the critical angle as determined by an angle scan such as the one in Fig. 1b and the

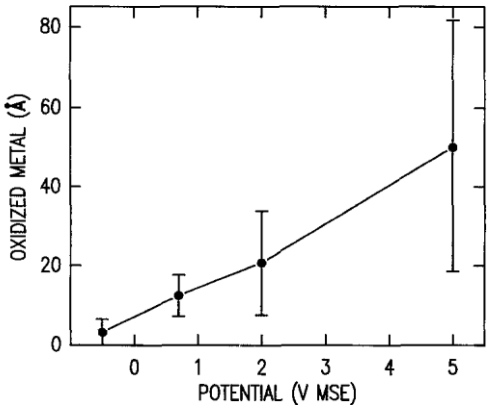

Fig. 16. Oxidized metal thickness as a function of applied potential for 20% Cr films determined by averaging the values of (fraction oxide × film thickness) at each potential in Fig. 5 for measurements made above the critical angle.

underlying Cr metal contributed to the signal. The fraction of the signal due to oxidized Cr thus decreased with increasing alloy layer thickness for measurements below as well as above the critical angle as shown in Fig. 5.

The thickness of metal oxidized in each film can be determined from Fig. 5 by the product of the fraction of oxidized Cr and the original alloy layer thickness, Fig. 16. While there is some scatter, the thickness of oxidized metal increases with potential at a rate of $\cong 9$ Å /V. The thickness for the oxide produced is greater than this value by a factor which depends upon the composition and density of the oxide. A factor of 1.28 is obtained assuming corundum ($A1_2O_3$) is formed and 3.2 for a hydrated oxide, gibbsite [$Al(OH)_3$] (26). These considerations suggest that the oxide thicknesses on the AlCr alloys are comparable to or greater than the conventional barrier oxide formed on Al of about 12 Å/V.

We have shown that the Cr(VI) is enriched at the oxide surface in contact with the electrolyte. It is of interest to know whether this Cr(VT) is actually part of the oxide or present as an adsorbed species. In an attempt to understand the nature of Cr(VI) in these oxides, we studied the response to subsequent potential changes. The effect of cathodic reduction is shown in Fig. 17 for the case of a 20% Cr, 40 Å sample that had been first polarized to 2 V. This high Cr composition sample exposed to a high potential exhibited a strong Cr(VI) signal. Following potentiostatic reduction of the same sample in the borate solution for 5 min at -1.5 V MSE, the pre-edge peak is almost totally absent, the edge is shifted to lower energy, and the near-edge features are indicative of the Cr(III) oxidation state. Subsequent reoxidation of the sample at 2 V

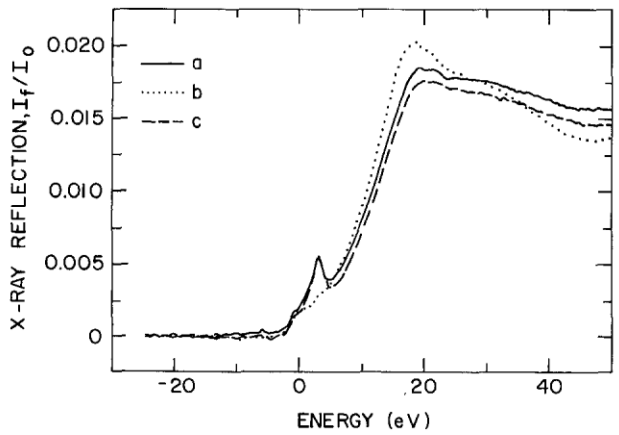

Fig. 17. Effect of reduction and reoxidation on 20% Cr 40 Å film measured above the critical angle, a, After first polarization at 2 V; b, after subsequent reduction at -1.5 V; and c, after second polarization at 2 V. Spectra not normalized to unit edge height.

resulted in an edge practically identical to the original one after the first polarization. The absorption edges in Fig. 17 were taken above the critical angle and thus represent the total Cr in the sample. Furthermore, these edges have not been normalized to unit height. As described above, there is some error inherent in this type of quantitative comparison for glancing angle conditions but efforts were made to reproduce conditions as closely as possible. By comparing the edges for the 2 V condition, Fig. 17 indicates that there is a only slight loss of Cr. This loss is less than the amount of Cr(VI) in the oxide which indicates that Cr(VI) is indeed reduced to Cr(III) during the reduction step. Interestingly, while the edge height decreases, the height of the pre-edge peak is the same indicating that the absolute amount of Cr(VI) is the same following the first and second oxidations. The same oxidation and reduction experiments have been repeated *in situ* and similar results were found (9, 10).

These experiments indicate that the chromate anions in the oxides are electrochemically active, capable of reversibly reducing and reoxidizing. This implies a reversible conversion between tetrahedral [Cr(VI)] and octahedral [Cr(III)] coordination.

The view that the Cr(VI) is incorporated into these oxides and not just adsorbed is fully supported by the analysis of Cr LVV Auger peaks that was published separately (11). This Auger line is much more sensitive than either XPS or XANES to the exact bonding structure of Cr(VI). Cr(VI) in oxides formed electrochemically on Al-Cr alloys was compared to Cr(VI) adsorbed from chromate solution onto anodized Al. The Cr(VI) adsorbed on the anodized Al behaved like chromate ion in that screening charge was easily transferred from the oxygen ligand in the final state of the photoemission process. This charge transfer from the ligand allowed the Cr LVV Auger transition to occur and the structure was susceptible to radiation-induced decomposition. On the other hand, for the Cr(VI) in oxides on AlCr alloys, screening charge is not readily transferred from the oxygen ligand. As a result of this and the fact that the d band for Cr(VI) is nominally empty, the Cr LVV Auger transition was not possible and was not observed. Correspondingly, Cr(VI) in the oxides on AlCr alloys did not readily suffer photodecomposition. This implies that the Cr—O bond for this Cr(VT) in the alloy oxide is affected by the influence of the second nearest neighbor, Al. As a result, the Cr(VI) behaves as if integrated into the oxide structure and is not isolated as chromate anions. This is consistent with the observation that the

Cr in the oxide is electroactive and can change coordination during oxidation and reduction cycles.

Both XPS and XANES indicated that the total amount of Cr(VI) which resides in the oxide at the interface with the electrolyte is invariant for an exposure time of 5 min. However, the *in situ* XANES experiments indicate that the proportion of Cr(VI) may change with time over a longer exposure period (10).

Conclusions

The behavior of Cr in oxide films electrochemically grown on AlCr alloys was studied by XANES and XPS. The following observations were made:

1. At potentials below the thermodynamically expected potential for the $C_2O_3/CrO^{\frac{2}{4}-}$ reaction, Cr in these oxide films was found to be only in the 3^+ oxidation state. Above this potential, both Cr(III) and Cr(VI) were observed. The Cr was almost all Cr(VI) for the thinnest films with high Cr concentrations polarized to the highest potential.
2. At a given potential, the proportion of Cr(VT) increased with Cr content in the alloy, probably as a result of band bending effects.
3. The Cr(VT) was concentrated in the outer part of the oxide film.
4. Cr(VI) in these oxides was electroactive in that it could be reversibly reduced to Cr(III). The Cr(VI) appeared to be present as part of the oxide lattice rather than as discrete adsorbed chromate ions.
5. The Cr/Al ratio in the oxides was independent of initial alloy concentration and equal to about 10% for a 5 min exposure time.

Acknowledgments

Research was carried out in part at the National Synchroton Light Source, Brookhaven National Laboratory, which is supported by the U.S. Department of Energy, Division of Materials Sciences and Division of Chemical Sciences. A. J. D. and H. S. I. were supported by the U.S. Department of Energy, Division of Materials Sciences, Office of Basic Energy Science under Contract No. DE-AC02-76CH00016. The authors are grateful to the personnel associated with beam lines X11A and X23A2 at the National Synchrotron Light Source for assistance in setting up the experiments and to Grant Coleman for help with the RBS analsyis. Helpful comments from the reviewers are also appreciated.

Manuscript submitted April 12, 1991; revised manuscript received Jan. 31, 1992. This was in part Paper 204 presented at the Montreal, Que., Canada, Meeting of the Society, May 6-11, 1991.

IBM T. J. Watson Research *Center assisted in meeting the publication costs of this article*.

REFERENCES

1. G. G. Long, J. Kruger, D. R. Black, and M. Kuriyama, *J. Electroanal. Chem.*, **150**, 603 (1983).
2. A. J. Forty, M. Kerkar, J. Robinson, and M. Ward, J. *Physiq.*, 47, C8-1077 (1986).
3. A. J. Davenport, H. S. Isaacs, and M. W. Kendig, *This Journal*, **136**, 1837 (1989).
4. A. J. Davenport and H. S. Isaacs, in "Surface and Inter-face Characterization in Corrosion," S. Shah, Editors, NACE, Houston, TX (1992).

5. J. K. Hawkins, H. S. Isaacs, S. M. Heald, J. Tranquada, G. E. Thompson, and G. C. Wood, *Corr. Sci.*, 27, 391 (1987).
6. S. W. M. Chung, J. Robinson, G. E. Thompson, G. C. Wood, and H. S. Isaacs, *Philos. Mag. B,* **63**, 557 (1991).
7. W. C. Moshier, G. D. Davis, and G. O. Cote, *This Journal*, **136**, 356 (1989).
8. G. S. Frankel, C. V. Jahnes, M. A. Russak, M. Mirzamaani, and V. A. Brusic, *ibid.*, **136**, 1243 (1989).
9. A. J. Davenport, H. S. Isaacs, G. S. Frankel, A. G. Schrott, C. V. Jahnes, and M. A. Russak, *ibid.*, **138**, 337 (1991).
10. A. J. Davenport, H. S. Isaacs, G. S. Frankel, A. G. Schrott, C. V. Jahnes, and M. A. Russak, in "X-ray Methods in Corrosion and Interfacial Electrochemistry," A. J. Davenport and J. G. Gordon, II, Editors, PV 92-1, p. 261, The Electrochemical Society Softbound Proceedings Series, Pennington, NJ (1992).
11. A. G. Schrott, G. S. Frankel, A.J. Davenport, H. S. Isaacs, C. V. Jahnes, and M. A. Russak, *Surf.* Sci, **250,**139 (1991).
12. F. W. Kutzler, C. R. Natoli, D. K. Misemer, S. Doniach, and K. O. Hodgson, *J. Chem. Phys.*, 73, 3274 (1980).
13. M. Kitamura, S. Muramatsu, and C. Sugiura, *Phys. Rev.* B, **33**, 5294 (1986).
14. T. Scimeca and G. Andermann, *Surf. Interface Anal.*, **15**, 235 (1990).
15. C. D. Wagner, "Practical Surface Analysis," D. Briggs and M. P. Seah, Editors, John Wiley & Sons, Inc., New York (1983).
16. D. A. Stephenson and N. J. Binkowski, J. *Non-Crystalline Sol*, **22,** 399 (1976).
17. R. Nyholm and N. Mortensson, J. *Phys. C,* **13**, L279 (1980).
18. C. J. Powell, *Surf. Sci.*, 44,29 (1974).
19. S. I. Raider and R. Flitsch, in "The Physics of $Si0_2$ and its Interfaces," S. Pantelides, Editors, Pergamon Press, Inc., New York (1978).
20. M. Pourbaix, "Atlas of Electrochemical Equilibria in Aqueous Solutions," Pergamon Press, Inc., New York (1966).
21. N. Sato, *Corr. Sci.*, **31**,1 (1990).
22. N. Sato, *This Journal*, **129**, 255 (1982).
23. X. Shangda, G. Changxin, L. Libin, and D. E. Ellis, *Phys. Rev. B*, **35**, 7671 (1987).
24. N. W. Ashcroft and N. D. Mermin, "Solid State Physics," Holt, Rinehart and Winston, New York (1976).
25. S. R. Morrison, "Electrochemistry at Semiconductor and Oxidized Metal Electrodes," Plenum Press, Inc., New York (1980).
26. "CRC Handbook of Chemistry and Physics," R. C. Weast, Editor, CRC Press, Cleveland, OH (1980).